Appl. Phys. B (2016) 122:197
DOI 10.1007/s00340-016-6474-0

Applied Physics B
Lasers and Optics

Large dynamic range optical vector analyzer based on optical single-sideband modulation and Hilbert transform

Min Xue[1] · Shilong Pan[1] · Yongjiu Zhao[1]

Received: 3 February 2016 / Accepted: 17 June 2016 / Published online: 29 June 2016

Abstract A large dynamic range optical vector analyzer (OVA) based on optical single-sideband modulation is proposed and demonstrated. By dividing the optical signal after optical device under test into two paths, reversing the phase of one swept sideband using a Hilbert transformer in one path, and detecting the two signals from the two paths with a balanced photodetector, the measurement errors induced by the residual −1st-order sideband and the high-order sidebands can be eliminated and the dynamic range of the measurement is increased. In a proof-of-concept experiment, the stimulated Brillouin scattering and a fiber Bragg grating are measured by OVAs with and without the Hilbert transform and balanced photodetection. Results show that about 40-dB improvement in the measurement dynamic range is realized by the proposed OVA.

1 Introduction

Many emerging applications, such as label-free single-molecule detection [1], on-chip signal processing [2], and laser interferometer space antenna [3], demand the optical devices having the capability to manipulate the optical spectrum with sub-MHz or even higher resolution. The Q-factor of the optical whispering-gallery-mode resonator can reach 6×10^{10} (corresponding to a 3-dB bandwidth of 3 kHz @ 1550 nm) [4], and the 3-dB bandwidth of the fiber Bragg grating (FBG) is as narrow as 9 MHz [5]. To obtain the spectral responses (i.e., magnitude, phase and polarization responses) of these devices, an optical vector analyzer (OVA) with ultrahigh resolution is essential. However, the conventional OVAs based on phase-shifted method [6] or interferometry approach [7] characterize the devices by scanning the wavelength of a laser. Restricted by the low wavelength accuracy of the wavelength-swept laser source, the resolution of these OVAs is too coarse to characterize high fineness spectrum manipulation optical devices [8].

To achieve the spectral responses with ultrahigh resolution, OVAs based on optical single-sideband (OSSB) modulation were developed [9–15]. Benefiting from the mature and ultrahigh-resolution microwave technologies, the resolution of the OSSB-based OVA can reach sub-hertz in theory [9] and 78 kHz in experiment [10]. However, the dynamic range is restricted by the measurement errors induced by the unwanted sidebands, including the residual −1st-order sideband and the high-order sidebands. Previously, an approach to eliminate the error induced by the unwanted −1st-order sideband was demonstrated [11], which reduces the measurement error by respectively measuring the devices using two OSSB signals with different SSRs and post-signal processing. Although the unwanted −1st-order-sideband-induced error is effectively suppressed, the approach is relatively complex and time consuming. It should be noted that the additional measurement error would be introduced if the spectral responses of the devices are drifted fast with time.

In this paper, a large dynamic range OSSB-based OVA employing optical Hilbert transform is proposed and demonstrated. By applying the proposed OSSB-based OVA, the unwanted-sideband-induced errors can be significantly reduced without two-step measurement and post-signal processing. In the scheme, the OSSB signal after an optical device under test (ODUT) is split into two parts. One part

✉ Shilong Pan
pans@ieee.org

[1] Key Laboratory of Radar Imaging and Microwave Photonics, Ministry of Education, Nanjing University of Aeronautics and Astronautics, Nanjing 210016, People's Republic of China

is directly introduced to one input port of a balanced photodetector (BPD), while the other part is sent to the BPD after propagating through an optical Hilbert transformer. By carefully adjusting the length and loss of the two paths, the two signals are simultaneously detected and vectorially subtracted in the BPD. Since the phase of the useful sideband in one path is reversed by the Hilbert transformer, the output photocurrent only contains the component beaten by the useful sideband and optical carrier, which is exactly the spectral responses of the ODUT.

2 Analytical analysis

Figure 1 shows the schematic diagram of the proposed OSSB-based OVA using an optical Hilbert transformer and a BPD. A laser diode (LD) outputs a continuous wave (CW), which is modulated by a RF signal from a RF source in an OSSB modulator. The optical field of the OSSB signal can be expressed as

$$\begin{aligned} E_{\mathrm{in}}(\omega) = {} & A_{-1} \times \delta[\omega - (\omega_o - \omega_e)] + A_0 \\ & \times \delta(\omega - \omega_o) + A_{+1} \times \delta[\omega - (\omega_o + \omega_e)] \\ & + \sum_{-\infty}^{n=-2} A_n \times \delta[\omega - (\omega_o + n\omega_e)] \\ & + \sum_{n=2}^{+\infty} A_n \times \delta[\omega - (\omega_o + n\omega_e)] \end{aligned} \tag{1}$$

where ω_o and ω_e are the angular frequencies of the optical carrier and the RF signal, respectively. A_n is the complex amplitude of the nth-order sideband.

When propagating through an ODUT, the magnitude and phase of the OSSB signal are changed accordingly. An optical splitter (OS) is used to divide the transmitted OSSB signal into two identical parts. One part is directly sent to one input port of a BPD (the upper path), and the other part is introduced to the other input ports after reversing the phase of the useful sideband in a Hilbert transformer

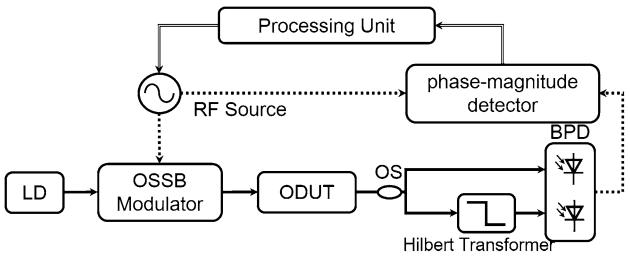

Fig. 1 Schematic diagram of the proposed OSSB-based OVA using an optical Hilbert transformer and a balanced photodetector. *LD* laser diode, *RF* radio frequency, *ODUT* optical device under test, *BPD* balanced photodetector, *OS* optical splitter

(the lower path). By balancing the upper and lower paths, the two paths have the identical length. Assuming that the phase of the positive order sidebands is exactly reversed, the optical fields of the two signals in the upper and lower paths can be written as

$$\begin{aligned} E_{\mathrm{U}}(\omega) = {} & B_{-1} \times \delta[\omega - (\omega_o - \omega_e)] + B_0 \times \delta(\omega - \omega_o) \\ & + B_{+1} \times \delta[\omega - (\omega_o + \omega_e)] \\ & + \sum_{-\infty}^{n=-2} B_n \times \delta[\omega - (\omega_o + n\omega_e)] \\ & + \sum_{n=2}^{+\infty} B_n \times \delta[\omega - (\omega_o + n\omega_e)] \end{aligned} \tag{2}$$

$$\begin{aligned} E_{\mathrm{L}}(\omega) = {} & B_{-1} \times \delta[\omega - (\omega_o - \omega_e)] + B_0 \times \delta(\omega - \omega_o) \\ & - B_{+1} \times \delta[\omega - (\omega_o + \omega_e)] \\ & + \sum_{-\infty}^{n=-2} B_n \times \delta[\omega - (\omega_o + n\omega_e)] \\ & - \sum_{n=2}^{+\infty} B_n \times \delta[\omega - (\omega_o + n\omega_e)] \end{aligned} \tag{3}$$

where $H(\omega) = H_{\mathrm{ODUT}}(\omega) \times H_{\mathrm{sys}}(\omega)$; $H_{\mathrm{ODUT}}(\omega)$ and $H_{\mathrm{sys}}(\omega)$ are the transmission functions of the ODUT and the measurement system, respectively. B_n is the complex amplitude of the nth-order sideband in the two paths.

In the BPD, the two signals are respectively converted into photocurrents. The electric field of the ω_e components is given by

$$\begin{aligned} i_{\mathrm{U}}(\omega_e) = {} & \eta B_0 B_{-1}^* H(\omega_o) H^*(\omega_o - \omega_e) \\ & + \eta B_{+1} B_0^* H(\omega_o + \omega_e) H^*(\omega_o) \\ & + \eta \sum_{\substack{n=-\infty \\ n\neq -1,0}}^{\infty} B_{n+1} B_n^* H[\omega_o + (n+1)\omega_e] H^*(\omega_o + n\omega_e) \end{aligned} \tag{4}$$

$$\begin{aligned} i_{\mathrm{L}}(\omega_e) = {} & \eta B_0 B_{-1}^* H(\omega_o) H^*(\omega_o - \omega_e) \\ & - \eta B_{+1} B_0^* H(\omega_o + \omega_e) H^*(\omega_o) \\ & + \eta \sum_{\substack{n=-\infty \\ n\neq -1,0}}^{\infty} B_{n+1} B_n^* H[\omega_o + (n+1)\omega_e] H^*(\omega_o + n\omega_e) \end{aligned} \tag{5}$$

where η is the responsivity of the BPD. On the right hand of Eqs. (4) and (5), the first terms and third terms are respectively the residual −1st-order-sideband-induced error and the high-order-sideband-induced errors, which are identical. The second terms represent the spectral responses of the ODUT, which are out of phase. At the output port of the BPD, these two photocurrents are vectorially subtracted. The electrical signal with the unwanted-sideband-induced errors removed is thus obtained,

$$i(\omega_e) = i_U(\omega_e) - i_L(\omega_e) = 2\eta B_{+1} B_0^* H(\omega_o + \omega_e) H^*(\omega_o) \quad (6)$$

To remove the transmission response of the measurement system, a calibration process can be performed, in which the ODUT is removed and the two test ports are directly connected, i.e., $H_{\mathrm{ODUT}}(\omega) = 1$. In this case, the transmission function of the measurement system, i.e., $H_{\mathrm{sys}}(\omega)$, can be acquired,

$$i_{\mathrm{sys}}(\omega_e) = 2\eta B_{+1} B_0^* H_{\mathrm{sys}}(\omega_o + \omega_e) H_{\mathrm{sys}}^*(\omega_o) \quad (7)$$

From Eqs. (6) to (7), we can obtain the accurate transmission response of the ODUT without the unwanted-sideband-induced errors, given by

$$H_{\mathrm{ODUT}}(\omega_o + \omega_e) = \frac{i(\omega_e) H_{\mathrm{ODUT}}^*(\omega_o)}{i_{\mathrm{sys}}(\omega_e)} \quad (8)$$

where $H_{\mathrm{ODUT}}^*(\omega_o)$ is a constant since it is the frequency response of the ODUT at a fixed wavelength.

3 Experiment results

To validate the capability of the unwanted-sideband-induced error suppression by the Hilbert transform and balanced photodetection, an experiment for stimulated Brillouin scattering (SBS) gain/absorption spectrum measurement is performed. Since the optical double-sideband (ODSB) signal has two equal sidebands, which would produce the largest unwanted-sideband-induced errors, we replace the OSSB modulator in Fig. 1 by a Mach–Zehnder modulator (MZM, Fujitsu) biased at the quadrature point. To excite the SBS effect in a 6-km single-mode fiber (SMF), a 1552.494-nm CW lightwave with a power of 16 dBm from a tunable laser source (TLS, Agilent N7714A) is split into two parts by an optical splitter. One part is amplified by an erbium-doped fiber amplifier (EDFA), which is used as the SBS pump. The other part is modulated by a RF signal from an electrical vector network analyzer (VNA, R&S ZVA67). After propagating through the 6-km single-mode fiber (SMF) and a circulator, the signal is divided into two parts. In the upper path, a tunable delay line and a tunable attenuator are inserted to balance the length and loss between the two paths. In the lower path, the phase of the useful sideband is reversed by a Hilbert transformer (Finisar WaveShaper 4000S). The WaveShaper 4000S is a programmable optical filter with full control of the filter amplitude and phase characteristics. A 50-GHz BPD (Finisar BPDV2150R) is employed to convert the two optical signals into a photocurrent. The optical spectra are measured by an optical spectrum analyzer (Yokogawa AQ6370C) with a resolution of 0.02 nm.

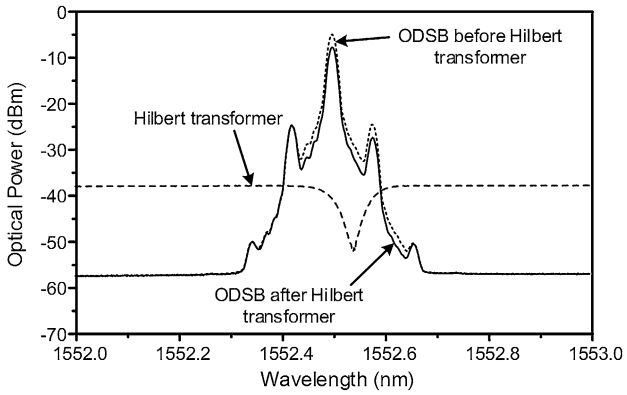

Fig. 2 Magnitude response of the Hilbert transformer and the optical spectra of the ODSB signals before and after the Hilbert transformer

Figure 2 shows the magnitude response of the Hilbert transformer and the optical spectra of the optical double-sideband (ODSB) signals before and after the Hilbert transformer. As can be seen, the optical carrier and the +1st-order sideband will be slightly attenuated by the stopband of the Hilbert transformer. With the increase of the RF frequency, the +1st-order sideband would be out of the stopband. In the experiment, the magnitude and phase responses of the SBS are characterized with a resolution of 100 kHz. Figure 3 shows the magnitude and phase responses of the SBS in the 6-km SMF measured by the ODSB-based schemes with and without the Hilbert transform and balanced photodetection, when the pump signal is set to have different powers. As shown in Fig. 3a, b, the magnitude and phase responses measured by the scheme without the Hilbert transform and balanced photodetection are the superposition of the gain spectrum and absorption spectrum. Therefore, there are two notches besides the gain peak, as shown in Fig. 3a. With the Hilbert transform and balanced photodetection, the influence of the absorption spectrum is eliminated, and the accurate gain spectrum and phase response in range of 700 MHz (10.3–11 GHz offset the optical carrier) are achieved, as shown in Fig. 3c, d, indicating that the unwanted-sideband-induced error is effectively suppressed.

To investigate the dynamic range improvement by the Hilbert transform and balanced photodetection, the OSSB-based OVA shown in Fig. 1 is constructed. The OSSB modulator is implemented by a dual-drive Mach–Zehnder modulator (DD-MZM, Fujitsu) and a 90-degree hybrid coupler (Krytar) [12]. Figure 4 shows the spectra of the modulated OSSB signals at different frequencies. The sideband suppression ratios (SSRs) of the OSSB signals are around 20 dB, as shown in the insert of Fig. 4. When the RF frequency is higher than 36 GHz, the SSR decreases with the frequency since the frequency range of the 90-degree hybrid coupler is 1.7-36 GHz.

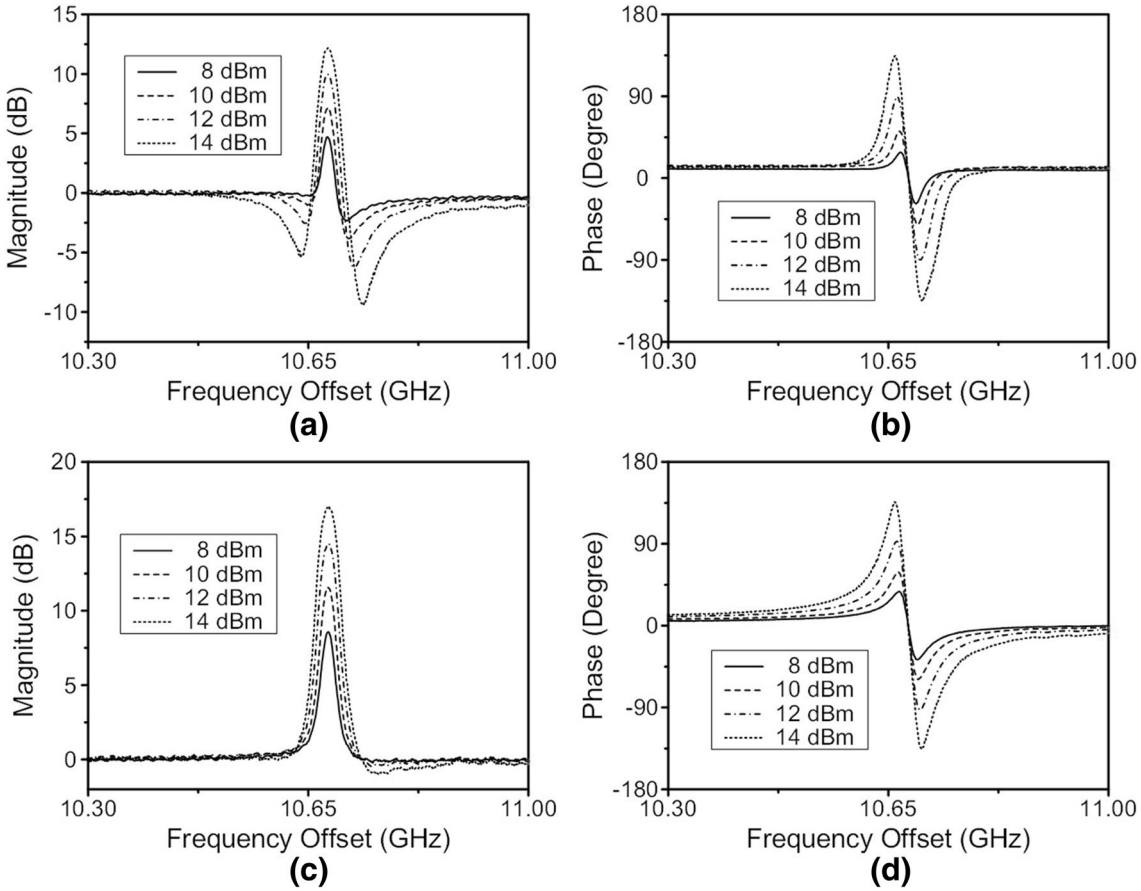

Fig. 3 Magnitude and phase responses measured by the ODSB-based schemes **a**, **b** without and **c**, **d** with the Hilbert transform and balanced photodetection

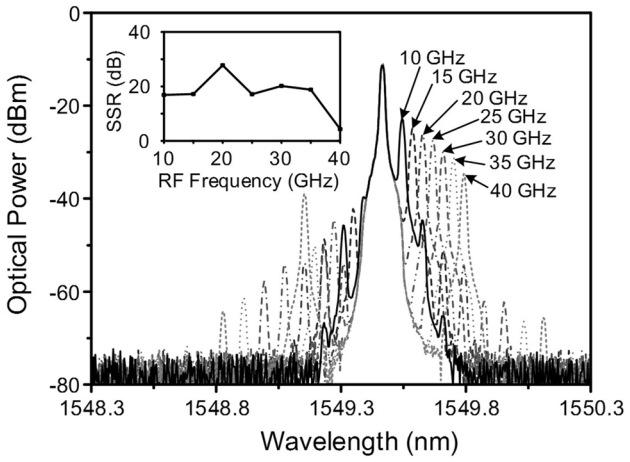

Fig. 4 Spectra of the OSSB signals with different RF frequencies. *Inset* SSR at different frequencies

Figure 5 shows the magnitude and phase responses of a fiber Bragg grating (FBG, TeraXion) measured by the conventional and the proposed OSSB-based OVAs with a resolution of 1 MHz. Since the SSR of the OSSB signal in conventional OSSB-based OVA is about 20 dB which is much smaller than the notch depth of the FBG, the measured magnitude and phase responses contain considerable errors induced by the unwanted sidebands, leading to a small dynamic range. On the other hand, when the proposed OVA is applied, the unwanted-sideband-induced errors are significantly suppressed and accurate responses are obtained, indicating that the dynamic range is greatly improved. It should be noted that the WaveShaper-based Hilbert transformer is only effective when the wavelength is far away from the optical carrier because the WaveShaper cannot achieve a sudden spectral-phase change. As a result, considerable measurement error would be present at the wavelength near the optical carrier.

In theory, the unwanted-sideband-induced errors can be ideally eliminated by carefully balancing the lengths and loss of the two paths. In practice, the imbalance of responsivity and uneven frequency response of the BPD must be considered. Figure 6 shows the frequency response of the BPD when two identical signals are

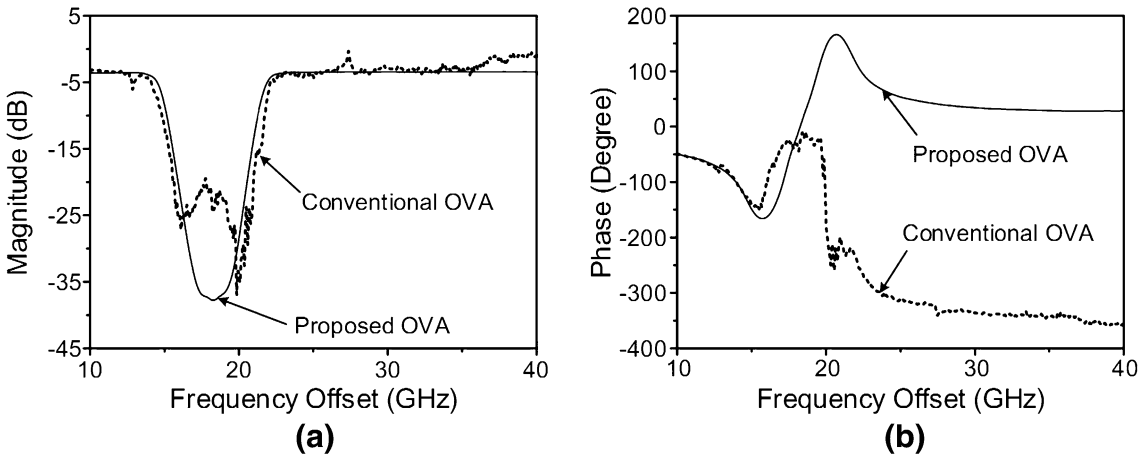

Fig. 5 **a** Magnitude and **b** phase responses measured by the conventional and the proposed OVAs

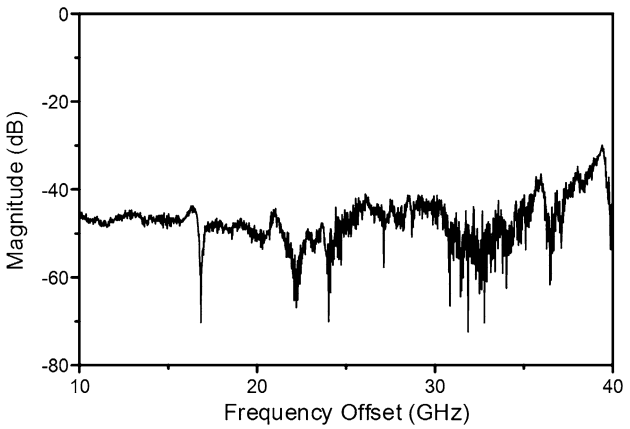

Fig. 6 Frequency response of the BPD when introducing two identical signals

respectively introduced to the two input ports. As can be seen, the RF common-mode rejection ratio (CMRR) of the BPD is larger than 40 dB, indicating that the residual unwanted-sideband-induced errors can be greatly suppressed and 40-dB dynamic range improvement can be achieved.

To evaluate the sensitivity of the CMRR on the loss mismatch and the phase difference between the two paths, a numerical simulation is performed. Figure 7 shows the CMRR as a function of the loss mismatch and the phase difference between the two paths. As can be seen, the CMRR decreases with the loss mismatch and the phase difference, which is 26.4 dB for a loss mismatch of 0.01 dB, while a 38.2-dB CMRR can be reached when the phase difference is 1 degree.

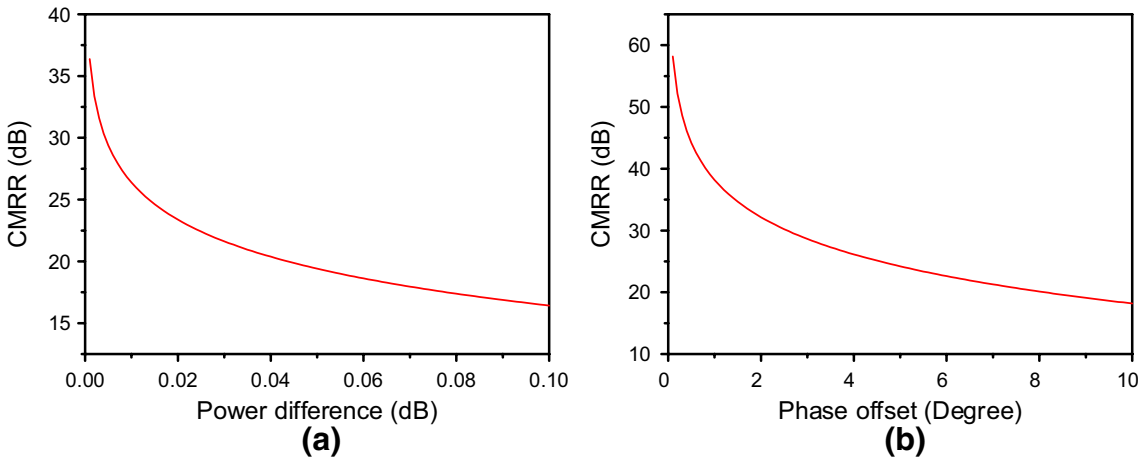

Fig. 7 Sensitivity of the CMRR as a function of **a** the loss mismatch and **b** the phase difference between the two paths

4 Conclusions

An OSSB-based OVA having a dynamic range improvement of ~40 dB as compared to the conventional OSSB-based OVA was proposed and demonstrated based on Hilbert transform and balanced photodetection. The experiment results show that the unwanted-sideband-induced errors can be greatly reduced and the dynamic range of the measurement is improved by about 40 dB.

Acknowledgments This work was supported in part by the National Natural Science Foundation of China (61527820, 61422108), the Jiangsu Provincial Program for High-level Talents in Six Areas (DZXX-034), the Fundamental Research Funds for the Central Universities, the Funding for Outstanding Doctoral Dissertation in NUAA (BCXJ13-08), and a Project Funded by the Priority Academic Program Development of Jiangsu Higher Education Institutions.

References

1. V. Kravets, F. Schedin, R. Jalil, L. Britnell, R. Gorbachev, D. Ansell, B. Thackray, K. Novoselov, A. Geim, A. Kabashin, Singular phase nano-optics in plasmonic metamaterials for label-free single-molecule detection. Nat. Mater. **12**(4), 304–309 (2013)
2. D.J. Moss, R. Morandotti, A.L. Gaeta, M. Lipson, New CMOS-compatible platforms based on silicon nitride and Hydex for nonlinear optics. Nat. Photonics **7**(8), 597–607 (2013)
3. T. Kessler, C. Hagemann, C. Grebing, T. Legero, U. Sterr, F. Riehle, M. Martin, L. Chen, J. Ye, A sub-s-mHz-linewidth laser based on a silicon single-crystal optical cavity. Nat. Photonics **6**(10), 687–692 (2012)
4. I.S. Grudinin, V.S. Ilchenko, L. Maleki, Ultrahigh optical Q factors of crystalline resonators in the linear regime. Phys. Rev. A **74**(6), 063806 (2006)
5. Y. Painchaud, M. Aubé, G. Brochu, M.-J. Picard, in *Bragg Gratings, Photosensitivity, and Poling in Glass Waveguides, OSA Technical Digest (CD)*. Ultra-narrowband notch filtering with highly resonant fiber Bragg gratings, paper BTuC3 (Karlsruhe, 2010)
6. T. Dennis, P. Williams, Achieving high absolute accuracy for group-delay measurements using the modulation phase-shift technique. IEEE J. Lightwave Technol. **23**(11), 3748–3754 (2005)
7. G.D. VanWiggeren, A.R. Motamedi, D. Barley, Single-scan interferometric component analyzer. IEEE Photonics Technol. Lett. **15**(2), 263–265 (2003)
8. http://www.lunatechnologies.com/products/ova/ova_main.html
9. J. Román, M. Frankel, R. Esman, Spectral characterization of fiber gratings with high resolution. Opt. Lett. **23**(12), 939–941 (1998)
10. Z. Tang, S. Pan, J. Yao, A high resolution optical vector network analyzer based on a wideband and wavelength-tunable optical single-sideband modulator. Opt. Express **20**(6), 6555–6560 (2012)
11. M. Wang, J. Yao, Optical vector network analyzer based on unbalanced double-sideband modulation. IEEE Photonics Technol. Lett. **25**(8), 753–756 (2013)
12. M. Xue, S.L. Pan, X.W. Gu, Y.J. Zhao, Performance analysis of optical vector analyzer based on optical single-sideband modulation. J. Opt. Soc. Am. B **30**(4), 928–933 (2013)
13. W. Li, J.G. Liu, N.H. Zhu, Optical vector network analyzer with improved accuracy based on polarization modulation and polarization pulling. Opt. Lett. **40**(8), 1679–1682 (2015)
14. M. Xue, S.L. Pan, Y.J. Zhao, Accurate optical vector network analyzer based on optical single-sideband modulation and balanced photodetection. Opt. Lett. **40**(4), 569–572 (2015)
15. M. Xue, S.L. Pan, Y.J. Zhao, Optical single-sideband modulation based on a dual-drive MZM and a 120-degree hybrid coupler. IEEE J. Lightwave Technol. **32**(19), 3317–3323 (2014)